THE JOURNAL OF PHYSICAL CHEMISTRY C

Article

pubs.acs.org/JPCC

# Theoretical Study of Hydrogen Adsorption on Ru-Decorated (8,0) Single-Walled Carbon Nanotube

Valeria Verdinelli,*[,†,§] Estefanía Germán,[‡] Carla R. Luna,[‡] Jorge M. Marchetti,[‡,§] María A. Volpe,[∥] and Alfredo Juan[‡]

[†]Departamento de Química and IFISUR, UNS-CONICET, Av. Alem 1253, 8000 Bahía Blanca, Argentina

[‡]Departamento de Física and IFISUR, UNS-CONICET, Av. Alem 1253, 8000 Bahía Blanca, Argentina

[§]Department of Mathematical Science and Technology, Norwegian University of Life Sciences, Drøbakveien 31, Ås, 1432, Norway

[∥]Departamento de Química and PLAPIQUI, UNS-CONICET, camino de La Carrindanga Km. 7, 8000 Bahía Blanca, Argentina

**ABSTRACT:** Hydrogen adsorption on Ru-decorated (8,0) zigzag single-walled carbon nanotube (SWCNT) was studied using density functional theory (DFT). Several decoration sites on the CNT surface were investigated before atomic or molecular hydrogen adsorption. The most stable location for a single Ru atom is above the hollow site, with an adsorption energy of $E_{ads}(Ru) = -2.133$ eV. Ru decoration increases hydrogen adsorption energy nearly 46% compared to pristine CNT. When a hydrogen molecule is considered on Ru/SWCNT its adsorption is dissociative with an $E_{ads}(H_2) = -0.697$ eV. The Ru-decorated SWCNT systems exhibit magnetic properties. Density of states (DOS) and overlap population density of states (OPDOS) were computed in order to study the evolution of the chemical bonding. C−C bonds interact with Ru and are weakened after adsorption. Strong Ru−H bonds are formed during hydrogen adsorption process at expenses of C−Ru bonds. The mains interactions include the Ru $5p_z$ and $4d_{z^2}$ and C $2p_z$ bands.

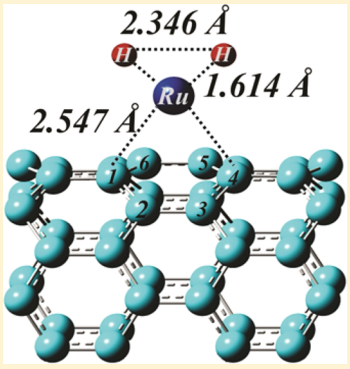


## 1. INTRODUCTION

Nowadays, hydrogen is one of the most promising clean energy carriers because of its abundance, environmental friendliness, high conversion efficiency and potentially abundant production from other renewable resources.[1−4] However, there are two important drawbacks in hydrogen utilization: production costs and storage characteristics.[5,6] Therefore, the key is developing secure and cheap storage technologies to save hydrogen.

Since their discovery by Iijima,[7] carbon nanotubes (CNT) have been the focus of extensive research both experimental and theoretical due to their fascinating physical and mechanical properties;[8−14] being considered potential candidates for hydrogen storage.[4,15−19] Previous experimental studies[20,21] have recognized that pristine single-walled (SW) CNTs have suitable hydrogen storage capacities at cryogenic temperatures due to their high surface-to-volume ratios. Unfortunately, the C−H interaction is too weak at room temperature and pressures.[22−24] Therefore, bare CNTs cannot store more than 1 wt % of hydrogen at these conditions and they are not practical for H storage.

Both experimental and theoretical studies have showed that carbon nanotubes turn more active for hydrogen adsorption at ambient conditions when they are doped with transition metal atoms (TM).

Only TM doping process preserves the structural integrity of carbon nanomaterials, and therefore, it can be considered as the best alternative for enhancing the hydrogen storage capacity. Extensive experimental research[25−35] has been performed to explain these phenomena. Zacharia et al.[29] reported that hydrogen storage capacity of Pd- and V-doped CNT at room temperature and at 2 MPa was nearly 30% more than purified CNT. In the same way, Suttisawat et al.[34] determined that at room temperature hydrogen adsorption capacity was 0.125 and 0.1 wt % for Pd-CNTs and V-CNTs, respectively. Ag-doped CNT enhances hydrogen adsorption more than 40% as compared to pristine CNT.[6] Recently, Rather et al.[35] found that Ni-decorated multiwalled carbon nanotube (MWCNT) improves hydrogen uptake capacity three times more than pristine MWCNT.

However, theoretical studies have shown that TM-doped CNTs improve $H_2$ adsorption.[36−46] Yildirim et al.[36] found that Ti atoms uniformly coated on nanotube surface could adsorb ∼8 wt % of $H_2$. They also report that SWCNT (12,0) doped with TM atoms such as V and Sc bound up five $H_2$ molecules.[41] Other research groups revealed that Ni-, Pd/Ni-, Pt-, and Pd-doped SWCNT have high hydrogen uptakes according to theoretical predictions.[39,40,42,43]

Recently, Seenithurai et al.[46] investigated $H_2$ adsorption on both Ni- and $NiH_2$-doped CNTs. They found that binding energy of five hydrogen molecules are stabilized on passivated Ni-doped CNT as well as they observed that desorption would take place above room temperature.

It is known that the development of air- and moisture-tolerant homogeneous Ru-based catalysts for alkene metathesis

**Received:** August 12, 2014
**Revised:** October 29, 2014
**Published:** November 7, 2014





dx.doi.org/10.1021/jp508183t | J. Phys. Chem. C 2014, 118, 27672−27680

has had a major impact in total synthesis and in materials chemistry.[47] Ruthenium is the most active metal for CO hydrogenation and production of long-chain hydrocarbons without any promoters.[48] Moreover, Ru catalysts show higher activity in ammonia synthesis and decomposition compared with other metal catalysts such as Ni, Fe, Rh, Pt, and Pd.[49] Ru and Ru alloy nanoparticles deposited on carbon based supports have recently drawn much attention for their long-term reactivity. Ru nanoparticles in ordered mesoporous carbon material and on carbon nanotubes showed higher catalytic activity in Fischer−Tropsch synthesis,[50,51] hydrogenation of glucose,[52] and ammonia decomposition.[53] It has been argued that the intimate contact of Ru nanoparticle with the carbon support enhance the hydrogen spillover and facilitated hydrogen dissociation on the catalyst surface.

Theoretical studies on Ru nanoparticles on SWCNT are rather scarce. In a related system, Liu et al.[54] suggested, from ab initio calculations, that $Ru_{13}$ nanoparticles deposited on defective graphene are expected to exhibit both high stability against sintering and superior catalytic performance in hydrogenation, oxygen reduction reaction, and hydrogen evolution reaction. Machado et al.[55] reported a comprehensive experimental and theoretical study of the surface chemistry of Ru nanoparticles supported on/in multiwalled carbon nanotubes (MWCNTs).

Regarding hydrogen storage properties of Ru-doped carbon materials, a few articles can be found in the open literature. Wang et al.[56] reported that hydrogen storage follows the sequence Ru/C > Pt/C > Ni/C on both templated carbon (TC) and superactived carbon at 298 K and 10.3 MPa. They also found that Ru nanoparticle-doped templated carbon by thermal reduction (Ru/TC-T) showed the highest hydrogen storage capacity at 298 K and 10.3 MPa.

There are other important materials where Ru plays a critical role, the Pt−Ru bimetallic catalysts. These materials are promising anodic catalysts for commercial direct methanol fuel cells (DMFC).[57] Alloying Pt with Ru improves significantly the resistance toward CO poisoning with respect to pure Pt, and the resistance increases with an increasing amount of Ru in the alloys.[58] The role of Ru in Pt−Ru/CNT materials at molecular level is far from being understood.[59,60] Harries et al.[61] reported DFT calculations of the anchoring of Pt and Pt/Ru to carbon nanofibers; however, they do not use single atoms or nanoparticles but bulk like alloys to represent the bimetallic catalyst.

To the best of our knowledge no calculations related to hydrogen uptake on a single Ru atom/SWCNT has been reported. The already mentioned unique chemical properties of Ru (and Ru−Pt alloys) supported on carbon-based materials deserves a detailed investigation that search about the nature of its electronic structure and chemical bonding. To achieve this goal we start from a single Ru atom deposited on pristine SWCNT, and then we consider H and $H_2$ adsorption on the supported metal particle. The system has been investigated using density functional theory (DFT). Geometrical structures, adsorption energies, and electronic properties have been studied. The electronic structure and bonding evolution have been analyzed using the concept of density of states (DOS) and overlap population (OPDOS) curves.

## 2. COMPUTATIONAL DETAILS

Spin-polarized density functional theory (DFT) simulations[62] were implemented using the Vienna ab initio simulation package (VASP).[63] The generalized gradient approximation (GGA) of Perdew−Burke−Ernzerhof (PBE)[64] and projector-augmented wave (PAW) pseudopotential[65,66] were set for the calculations. A plane-wave basic set with a cutoff energy of 700 eV was adopted for all calculations. The Brillouin-zone of the supercell was sampled by (1 × 5 × 1) *k*-points within Monkhorst−Pack scheme.[67] Test calculations have shown that including more *k*-points does not affect the results. van der Waals corrections described by DFT-D2 method of Grimme[68] were included.

A semiconducting (8,0) zigzag SWCNT modeled by a 20 × 8.52 × 20 $Å^3$ supercell containing 64 C atoms was chosen as model system.[69] The separation along the *x* and *z* directions are large enough to avoid interactions among adsorbates and among CNT images. To minimize the computational cost we relaxed the first and second neighbors, while the remaining C atoms were kept fixed to the initial positions. The total energy convergence and the forces on the atoms were less than $10^{-4}$ eV and 0.01 eV/Å, respectively. Self-consistent calculations were considered to converge when the difference in total energy between consecutive steps did not exceed $10^{-5}$ eV. In addition, static calculations were considered to converge using the same criterion.

Four possible decoration sites on CNT surface were considered (i.e., the Ho site above the C-hexagon, the Z and A sites above zigzag and axial C−C bonds, and the T site above the carbon atom) as described in Figure 1.

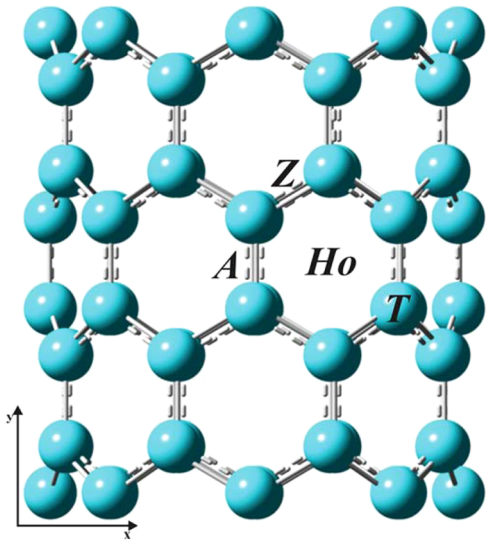


**Figure 1.** Schematic description of different adsorption sites on a zigzag (8,0) CNT: Ho, hollow; A, axial; Z, zigzag; T, top.

Adsorption energies were calculated according to the following expression:

$$E_{ads}(X) = E_{(X/SWCNT)} - E_{(X)} - E_{(SWCNT)} \quad (1)$$

where $E_{(X/SWCNT)}$ is the total energy of the adatom X adsorbed on SWCNT, $E_{(SWCNT)}$ is the energy of the bare SWCNT, $E_{(X)}$ is the energy of a free adsorbate X.

However, adsorption energies of hydrogen atom and hydrogen molecule on the Ru-doped-SWCNT was obtained from

$$E_{ads}(H) = E_{(H-Ru/SWCNT)} - E_{(H)} - E_{(Ru/SWCNT)} \quad (2)$$


dx.doi.org/10.1021/jp508183t | J. Phys. Chem. C 2014, 118, 27672−27680

$$E_{ads}(H_2) = E_{(H2-Ru/SWCNT)} - E_{(H2)} - E_{(Ru/SWCNT)} \quad (3)$$

where $E_{(H-Ru/SWCNT)}$ and $E_{(H2-Ru/SWCNT)}$ are the total energy of H and total energy of $H_2$ adsorbed on Ru/SWCNT system, $E_{(Ru/SWCNT)}$ is the total energy of the decorated SWCNT system, and $E_{(H)}$ and $E_{(H2)}$ are the energy of a free H atom and $H_2$ molecule, respectively.

To analyze the electronic structure and bonding we have used the concept of density of states (DOS) and overlap population (OP)[70−74] to shed more light on the C−Ru−H interaction. The DOS curve is a plot of the number of orbitals per unit volume per unit energy. The OPDOS curve is a plot of the overlap population weighted DOS vs energy. Integration of the OPDOS curve up to the Fermi level ($E_F$) gives the total overlap population of the specified bond. Looking at the OPDOS, we may analyze the extent to which specific states contribute to a bond between atoms or orbitals.[74] The OP and OPDOS curves were calculated using the Amsterdam density functional (ADF) code.[75] A similar analysis was reported by Luna et al.[76] and Lopez-Corral et al.[77]

## 3. RESULTS AND DISCUSSION

**3.1. Addition of Hydrogen to Bare Ru Atom: H−Ru and $H_2$−Ru Systems.** As a previous study we analyzed the interaction between H atom and Ru atom as well as the interaction between $H_2$ and Ru atom. In the first case the Ru−H bond length was 1.596 Å with a binding energy (BE) of 2.82 eV (see Table 1 and Figure 2). In the second case the $H_2$ molecule was located in three different adsorption sites, as we can see in Figure 2. Among these, configuration (*III*) is energetically the most stable, BE = 1.25 eV, with a H−H distance of 1.908 Å, indicating that the hydrogen is adsorbed dissociatively like on bulk surfaces[78] and small TM clusters.[79,80] These results agree with previous studies of $H/H_2$ adsorption on TM.[37,81−83] Wang et al.[84] reported Ru−H and Ru−$H_2$ bond lengths similar to those listed in Table 1.

**Table 1. Equilibrium Bond Distances, Binding Energies (BE), and Total Magnetic Moment ($m$) after H and $H_2$ Adsorption on Bare Ru Atom**

| bond | bond distance (Å) | BE (eV) | $m$ ($\mu_B$) |
|---|---|---|---|
| H−H | 0.750[a] | 4.538[a] | 0.00 |
| Ru−H | 1.596 | 2.820[c] | 3.00 |
| H−Ru−H (I)[b] | 1.757 | −0.075[d] | 4.00 |
| Ru−H−H (II)[b] | 2.186 ($d_{H-H}$ = 0.769) | −0.512[d] | 4.00 |
| H−Ru−H (III)[b] | 1.579 ($d_{H-H}$ = 1.908) | 1.252[d] | 2.00 |

[a]These values are in fairly good agreement with experimental[85] and theoretical calculations.[69] [b]See Ru−$H_2$ systems labeling in Figure 2. [c]BE(H) = $E$(Ru) + $E$(H) −$E$(Ru−H). [d]BE($H_2$) = $E$(Ru) + $E$($H_2$) − $E$(Ru−$H_2$).

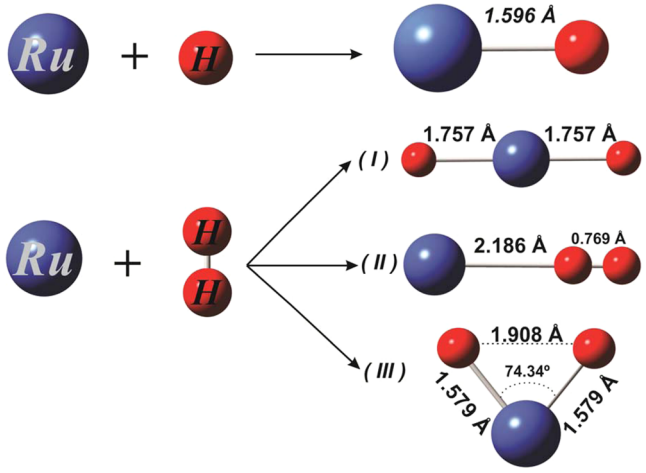


**Figure 2.** Optimized structures for H−Ru and $H_2$−Ru systems.

**3.2. Ru/SWCNT System.** The Ru adsorption on SWCNT was studied taking into account four different active sites: Z and A sites above the zigzag and axial C−C bonds, T site on top of the carbon atom, and the Ho site above the C-hexagon. Ru atom prefers to be near Ho site, with a calculated adsorption energy of −2.133 eV (see Figure 3a). Similar results were reported for other TM adsorption by Durgun et al.[86]

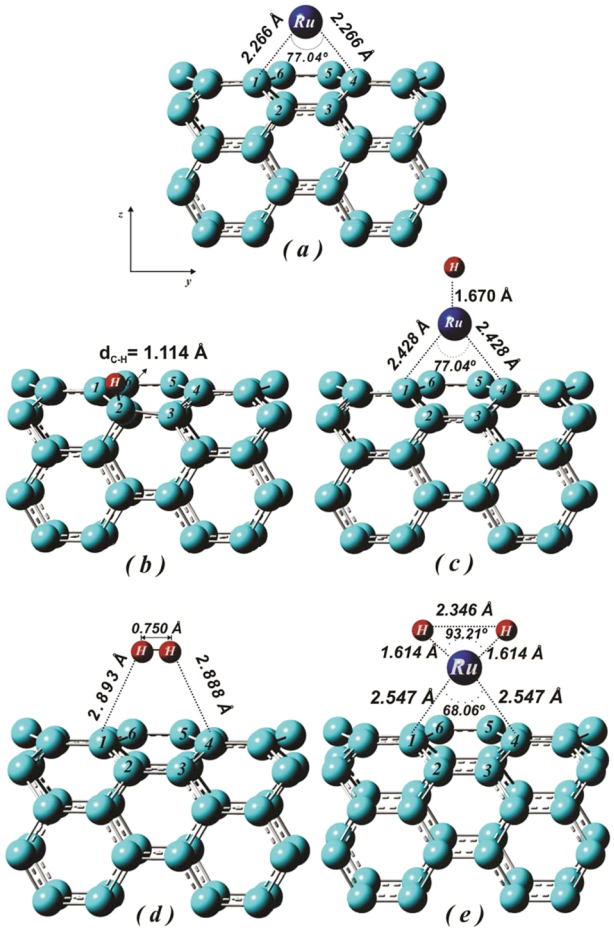


**Figure 3.** Optimized structures of (a) Ru-decorated CNT, (b) H atom on CNT, (c) H atom on Ru/CNT, (d) $H_2$ molecule on CNT, and (e) $H_2$ molecule on Ru/CNT at the most stable site.

The optimized bond lengths and OP values for pristine, decorated CNT and all adsorption systems are listed in Table 2. After Ru adsorption, C−Ru bonds are originated with bond lengths and OP values of 2.266 Å and 0.164, respectively. Liu et al.[54] computed the minimun Ru−C distance for $Ru_{13}$/graphene and found a value of 2.20 Å with a binding energy of −2.45 eV. It can be seen also in Table 2, that C−C bonds near Ru adsorption site elongate 2% and their strength decrease between 4 and 8%. C1 and C4 atoms participate in the bonding process mainly by their $2p_z$ orbitals and their orbital


dx.doi.org/10.1021/jp508183t | J. Phys. Chem. C 2014, 118, 27672−27680

Table 2. Bond Distances ($d$) and Overlap Population (OP) for Optimized Pristine CNT and Ru−CNT Systems[a]

| | $CNT_{bare}$ | | Ru−CNT | | H−Ru/CNT | | H−H[b] | | $H_2$−Ru/CNT | |
|---|---|---|---|---|---|---|---|---|---|---|
| bond | $d$ (Å) | OP | $d$ (Å) | OP | $d$ (Å) | OP | $d$ (Å) | OP | $d$ (Å) | OP |
| C1−C2 | 1.434 | 0.984 | 1.461 | 0.940 | 1.459 | 0.949 | | | 1.445 | 0.956 |
| C2−C3 | 1.417 | 1.033 | 1.407 | 1.053 | 1.405 | 1.052 | | | 1.417 | 1.043 |
| C3−C4 | 1.434 | 0.984 | 1.461 | 0.940 | 1.459 | 0.949 | | | 1.445 | 0.956 |
| C4−C5 | 1.434 | 0.984 | 1.469 | 0.904 | 1.465 | 0.915 | | | 1.462 | 0.891 |
| C5−C6 | 1.417 | 1.033 | 1.436 | 0.976 | 1.440 | 0.976 | | | 1.444 | 0.973 |
| C6−C1 | 1.434 | 0.984 | 1.469 | 0.904 | 1.465 | 0.915 | | | 1.462 | 0.891 |
| Ru−C1 | | | 2.266 | 0.164 | 2.428 | 0.113 | | | 2.547 | 0.111 |
| Ru−C4 | | | 2.266 | 0.164 | 2.428 | 0.113 | | | 2.547 | 0.111 |
| Ru−C5 | | | 2.127 | 0.151 | 2.188 | 0.151 | | | 2.150 | 0.197 |
| Ru−C6 | | | 2.127 | 0.151 | 2.188 | 0.151 | | | 2.150 | 0.197 |
| H−H | | | | | | | 0.750 | 0.802 | 2.346 | 0.018 |
| H−Ru | | | | | 1.670 | 0.702 | | | 1.614 | 0.643 |
| H−C5 | | | | | 3.740 | 0.000 | | | 2.903 | 0.004 |
| H−C6 | | | | | 3.740 | 0.000 | | | 2.903 | 0.004 |

[a]The atom labeling is indicated in Figure 3. [b]Gas phase.

Table 3. Electron Orbital Occupations for Optimized Pristine Ru−CNT, H−Ru/CNT, and $H_2$−Ru/CNT Systems

| | s | $p_x$ | $p_y$ | $p_z$ | $d_{x^2-y^2}$ | $d_{z^2}$ | $d_{xy}$ | $d_{xz}$ | $d_{yz}$ |
|---|---|---|---|---|---|---|---|---|---|
| Ru Atom | | | | | | | | | |
| Ru | 0.000 | 0.000 | 0.000 | 0.000 | 1.600 | 1.600 | 1.600 | 1.600 | 1.600 |
| $CNT_{pristine}$ | | | | | | | | | |
| C | 1.140 | 0.931 | 0.931 | 0.990 | | | | | |
| CNT−Ru | | | | | | | | | |
| C | 1.157 | 0.939 | 0.917 | 0.928 | | | | | |
| Ru | 0.307 | 0.103 | 0.268 | 0.000 | 1.958 | 1.980 | 1.952 | 1.926 | 1.924 |
| CNT/Ru−H | | | | | | | | | |
| C | 1.156 | 0.940 | 0.924 | 0.936 | | | | | |
| Ru | 0.701 | 0.092 | 0.195 | 0.303 | 1.984 | 1.908 | 1.965 | 1.926 | 1.945 |
| H | 1.298 | | | | | | | | |
| CNT/Ru−$H_2$ | | | | | | | | | |
| C | 1.149 | 0.941 | 0.915 | 0.849 | | | | | |
| Ru | 0.595 | 0.067 | 0.359 | 0.335 | 1.973 | 1.967 | 1.927 | 1.925 | 1.465 |
| H | 1.101 | | | | | | | | |

occupation decrease 6.20% after Ru adsorption. TM atom interacts mainly with its $4d_{z^2}$ orbitals as can be seen in Table 3.

The OPDOS curves in Figure 4a plots Ru−C interactions after Ru adsorption on CNT, while Figure 4b shows C−C interactions before and after Ru atom adsorption. It can be seen that C−C and Ru−C interactions are mainly bonding (the area of the curves below the Fermi level in the bonding half region is large). As it is usual in these plots, contributions above the horizontal axis are bonding between atoms, while contributions below are antibonding. Also, it can be noticed that C−C OPDOS area decreases after Ru adsorption due to the formation of Ru−C bond.

Figure 5 shows the electronic structure (DOS) of (a) pristine and (b) Ru atom adsorbed on the CNT. The blue tick marks in the DOS plot represents the electronic levels of isolated Ru atom before adsorption.

It can be observed that ruthenium adsorption reduces CNT energy gap from 0.58 to 0.40 eV, this lower value is due to the interaction of C with Ru that decreases the cohesion energy of the SWCNT. Pristine (8,0) band gap energy of 0.58 eV was reported by Karami Horastani et al.[87] The Fermi level ($E_F$) is placed immediately above the valence band, and this band spreads out about −8 eV and presents several sharp peaks. The main contribution of Ru is located in the conduction band.

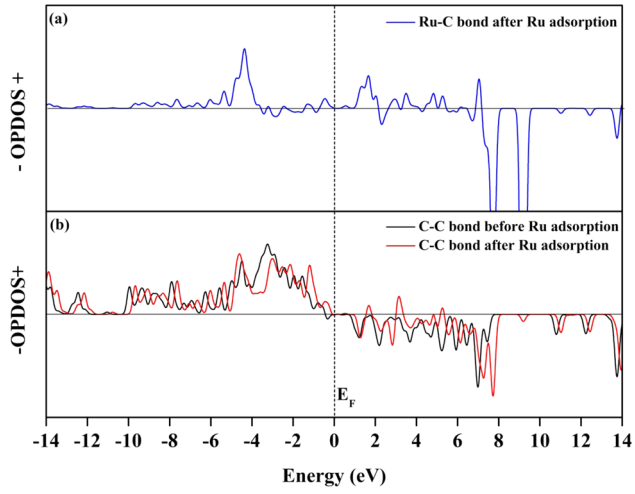


Figure 4. OPDOS curves of selected bonds: (a) Ru−C formed bond and (b) C−C before and after the Ru adsorption on SWCNT.

**3.3. H/Ru/SWCNT System.** Previous studies have reported[86−88] that the top site is the most stable configuration of H atom adsorbed on pristine SWCNT with a C−H bond length of 1.114 Å as is shown in Figure 3b.


dx.doi.org/10.1021/jp508183t | J. Phys. Chem. C 2014, 118, 27672−27680

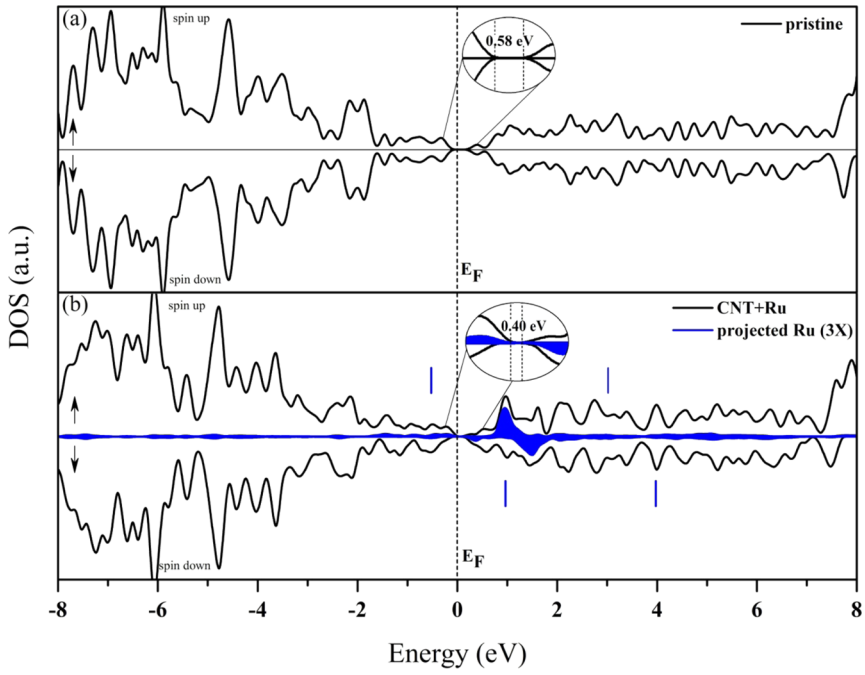


**Figure 5.** DOS curves for (a) pristine CNT and (b) Ru adsorption on CNT. The tick marks indicate free Ru atom energy levels. The projected DOS of adsorbed Ru is shaded in blue.

**Table 4. Adsorption Energies ($E_{ads}$), Bond Distances, Total Magnetic Moment ($m$), and Band Gap Energies ($E_g$) for Pristine CNT, H−CNT, Ru−CNT, and H−Ru/CNT Systems**

| | $CNT_{pristine}$ | H−CNT | Ru−CNT | H−Ru/CNT | $H_2$−CNT | $H_2$−Ru/CNT |
|---|---|---|---|---|---|---|
| $E_{ads}$ (eV) | | −1.595 | −2.133 | −2.330 | −0.051 | −0.697 |
| $d_{C-C}$ (Å)[a] | 1.417 | 1.397 | 1.407 | 1.405 | 1.416 | 1.417 |
| | 1.434 | 1.523 | 1.469 | 1.465 | 1.434 | 1.462 |
| $d_{C-Ru}$ (Å) | | | 2.266 | 2.428 | | 2.547 |
| $d_{C-H}$ (Å) | | 1.114 | | | 2.890 | |
| $d_{Ru-H}$ (Å) | | | | 1.670 | | 1.610 |
| $m$ ($\mu_B$) | 0.00 | 1.00 | 2.00 | 3.00 | 0.00 | 2.00 |
| $E_g$ (eV) | 0.58 | 0.34 | 0.40 | 0.43 | 0.58 | 0.44 |

[a]C−C distances for C−C bonds first and second neighbor to adsorbed species, respectively.

When a H atom is adsorbed on Ru-decorated CNT, it is located on top of Ru (Ru−H bond length = 1.670 Å) (see Figure 3). Adsorption energies calculated as eq 1 are given in Table 4 as well as geometry data for all studied systems. The H adsorption energy is improved from −1.595 eV (on pristine SWCNT) to −2.330 eV on Ru-decorated SWCNT. Similar results have been reported by Tabtimsai et al.[45] and Reyhani et al.[89] who observed that hydrogen storage capacity was increased in decorated CNTs by Fe, Ca, Co, Ni, and Pd compared to pristine CNT.

It can be noticed that C−Ru distances increase by 7% and Ru−H distance is incremented from 1.596 Å (free Ru−H molecule) to 1.670 Å (H−Ru/SWCNT system). At the same time, decorated CNT systems present magnetic moments, while bare SWCNT (8.0) shows a nonmagnetic ground state. These results are in agreement with theoretical calculations by Durgun et al.[90] who found that most of the TM atom adsorbed on (8,0) SWCNT presents an important magnetic moment.

OP values for C−C, C−Ru, H−H, and H−Ru in all analyzed systems are listed in Table 2. The results show that OP value for the Ru−H bond is 0.702, while there is no C−H OP in Ru-decorated CNT system. At the same time, it can be seen that OP for the Ru−$C_1$ and Ru−$C_4$ bonds decrease 31%, whereas OP values for Ru−$C_5$ and Ru−$C_6$ bonds are not affected after H atom adsorption.

Regarding the Ru−H, Ru−C, and C−C OPDOS curves, no significant changes were found after H atom adsorption.

In Figure 6 we can see a shift of the orbital bands of Ru toward the valence band, as well as H energetic state making the system more stable (gap from 0.40 to 0.43 eV). Also we can notice the spreading out of the bands due to the strong interaction of Ru with H; the d-states of TM are strongly hybridized with the s state of H atom. Moreover, we can observe that after H adsorption on Ru/CNT the system is half-metallic (see the magnified region near $E_F$ in Figure 6).

**3.4. $H_2$/Ru/SWCNT System.** In the case of $H_2$ on bare SWCNT, it was found that the most stable location is on the center of a C-hexagon with C−H distances and adsorption energy of about 2.890 Å and −0.051 eV, respectively. Moreover, it is shown in Figure 3d that the effect of adsorption on H−H bond length (0.750 Å) is negligible. These values are in good agreement with previous studies.[37,87,91]

When the hydrogen molecule is adsorbed on Ru-decorated (8,0) CNT, adsorption energy is enhanced from −0.051 eV ($H_2$−CNT) to −0.697 eV ($H_2$−Ru/CNT), whereas the H−H bond elongates and it finally became dissociative. Dag et al.[37]


dx.doi.org/10.1021/jp508183t | J. Phys. Chem. C 2014, 118, 27672−27680

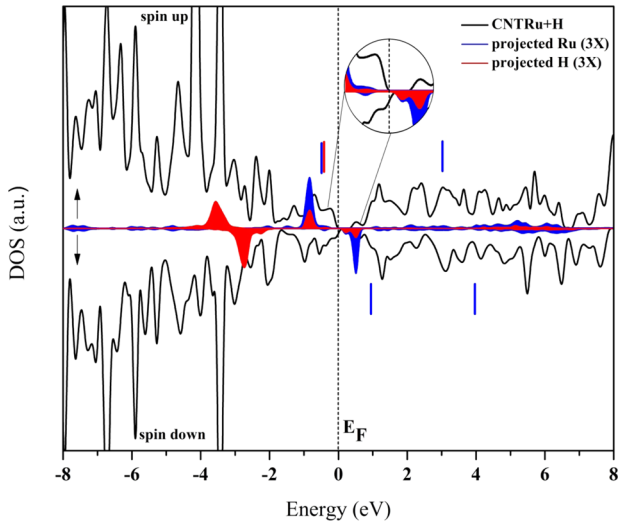


**Figure 6.** DOS curves for H adsorption on Ru-doped-SWCNT. The tick marks indicate free Ru atom and H atom. The projected DOS of adsorbed Ru and adsorbed H are shaded in blue and red, respectively.

have also reported that a $H_2$ molecule is dissociatively adsorbed ($d_{H-H}$ = 1.86 Å) on a single Pt atom at the hollow site of SWCNT. At this point, H−H bond is weakened and its length increases from 0.750 to 2.346 Å. The H−H OP (see Table 2) changes from 0.802 to 0.018 on Ru/CNT. The s electron of hydrogen slightly hybridizes with d orbital of Ru, which weakens the interactions between Ru and C (see Table 3). Thus, Ru−$C_1$ and Ru−$C_4$ distances elongate from 2.266 to 2.547 Å with an OP value of 0.111. Furthermore, C1−Ru−C2 angle decreased from 77.04° to 68.0°, and H−Ru−H angle increased by 25% when compared with Ru−$H_2$ molecule (see Figure 3e).

The evolution of the chemical bond was examined through the analysis of OP values and OPDOS curves for selected bonds. Table 2 revels that OP values for Ru−$C_1$ and Ru−$C_4$ are weakened approximately 32%. Table 2 shows an important OP change in the H−H bond, from 0.802 to 0.018 after adsorption, demonstrating the strong interaction of $H_2$ with the system.

As it can be observed in Figure 7, Ru−H, C−H, H−H, C−C, and Ru−C interactions are mainly bonding, only OPDOS curves of C−H (Figure 7a), H−H (Figure 7b), and Ru−C (Figure 7d) present slight antibonding areas after $H_2$ molecule adsorption. C−C remains almost the same (see Figure 7c), and from Ru−C we can see the weakening of Ru−C bond after adsorption because the curve is mostly in the antibonding side and the area under the $E_F$ decreases in comparison with the curve before $H_2$ adsorption. The H−H bond OPDOS curve before adsorption is sharp and well-defined, but after adsorption it spreads out due to the interaction of 1s orbitals of H and $4d_{z^2}$ and $5p_z$ of Ru.

The OP values corresponding to the new bonds originated during adsorption process are also present in Table 2. Thus, OP values of the formation of Ru−H bonds are 0.643, while OP values for C−H bonds are 0.004, indicating that Ru−H interaction is stronger than C−H interaction (see Figure 7a).

In Figure 8, the projection of Ru and $H_2$ DOS curves are even more spread out than the single H adsorption system. The main peaks are shifted to the valence band, with notorious hybridization of d-bands of Ru and s-bands of $H_2$ between −4 and −2 eV.

## 4. CONCLUSIONS

In this work, hydrogen adsorption on Ru-decorated CNT was examined using spin-polarized density functional theory (DFT)

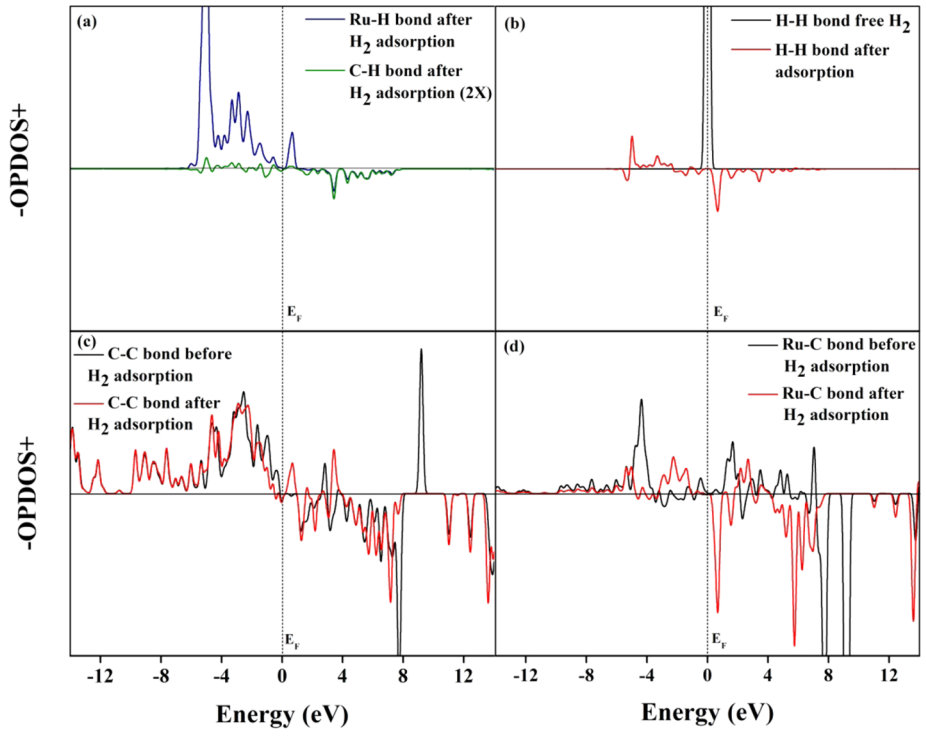


**Figure 7.** OPDOS curves of selected bonds: (a) Ru−H and C−H formed bonds, (b) H−H before and after $H_2$ adsorption on Ru−CNT, (c) C−C before and after $H_2$ adsorption on Ru−CNT, and (d) Ru−C before and after $H_2$ adsorption on Ru−CNT.


dx.doi.org/10.1021/jp508183t | J. Phys. Chem. C 2014, 118, 27672−27680

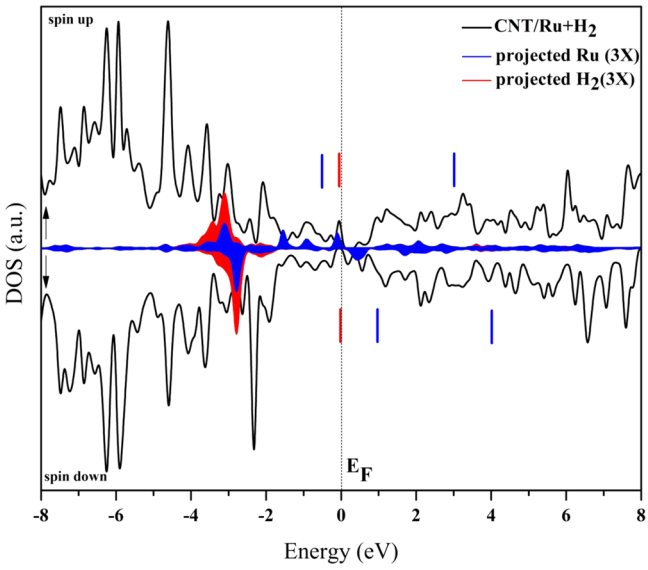


**Figure 8.** DOS curves for $H_2$ adsorption on Ru-decorated-SWCNT. The tick marks indicate free Ru atom and $H_2$ molecule. The projected DOS of adsorbed Ru and adsorbed $H_2$ molecule are shaded in blue and red, respectively.

calculations. Ru atom prefers to be near the hollow site on the CNT with Ru−C bond lengths of 2.266 Å. When a H atom adsorbed on Ru-decorated CNT is located on the top of Ru, C−Ru distances increase by 7% and Ru−H distance is incremented from 1.596 Å (free Ru−H molecule) to 1.670 Å (H−Ru/SWCNT system). Whereas a hydrogen molecule is adsorbed on Ru-decorated CNT, the H−H bond elongates from 0.750 to 2.346 Å. The C−Ru−C angle decreases from 77.0° to 68.0°, and the H−Ru−H angle increases by 25% when it is compared with Ru−$H_2$ molecule.

However, a TM atom induces a magnetic ground state when it is adsorbed on (8,0) SWCNT and reduces its energy gap from 0.58 to 0.40 eV. Furthermore, Ru-decorated CNT enhances hydrogen adsorption. This energy changes from −1.595 eV (on pristine CNT) to −2.330 eV. Hydrogen molecule adsorption on Ru-doped CNT is dissociative with an $E_{ads}$ = −0.697 eV, resulting in an improvement of $H_2$ adsorption compared with that on pristine CNT. These adsorption processes take place by interaction of H−Ru−C. H interacts with its 1s orbital, Ru mainly with $5p_z$ and $4d_{z^2}$, and C with $2p_z$ because these orbitals are perpendicular to the surface and it is easier to overlap with the adsorbates.

## AUTHOR INFORMATION

### Corresponding Author

*Tel: +54-291-4882982. Fax: +54-9-291-4595142. E-mail: vverdinelli@uns.edu.ar.

### Notes

The authors declare no competing financial interest.

## ACKNOWLEDGMENTS

We acknowledge the financial support given by SGCyT-UNS, PICT-2010-1770, PICT-2012-1609, PIP No. 112-200801-01440, Res. 4541/12 and 774/13, Comisión de Investigaciones Científicas-BA, and Research Council of Norway (YGGDRASIL grant No. 227272/F11). V.V., E.G., C.R.L., J.M.M., A.J., and M.A.V. are members of CONICET.

## REFERENCES

(1) Wang, H.; Takenaka, S.; Otsuka, K. Hydrogen Storage Properties of Modified Fumed-Fe-Dust Generated from a Revolving Furnace at a Steel Industry. *Int. J. Hydrogen Energy* **2006**, *31*, 1732−1746.

(2) Li, W.; Wang, H.; Ren, Z.; Wang, G.; Bai, J. Co-Production of Hydrogen and Multi-Wall Carbon Nanotubes from Ethanol Decomposition over $Fe/Al_2O_3$ Catalysts. *Appl. Catal., B* **2008**, *84*, 433−439.

(3) Gayathri, V.; Devi, N. R.; Geetha, R. Hydrogen Storage in Coiled Carbon Nanotubes. *Int. J. Hydrogen Energy* **2010**, *35*, 1313−1320.

(4) Ioannatos, G. E.; Verykios, X. E. $H_2$ Storage on Single- and Multi-Walled Carbon Nanotubes. *Int. J. Hydrogen Energy* **2010**, *35*, 622−628.

(5) Coontz, R.; Hanson, B. Not So Simple. *Science* **2004**, *305*, 957.

(6) Rather, S. U.; Naik, M. U. D.; Hwang, S. W.; Kim, A. R.; Nahm, K. S. Room Temperature Hydrogen Uptake of Carbon Nanotubes Promoted by Silver Metal Catalyst. *J. Alloys Compd.* **2009**, *475*, L17−L21.

(7) Iijima, S. Helical Microtubules Of Graphitic Carbon. *Nature* **1991**, *354*, 56−58.

(8) Dai, H. Carbon Nanotubes: Opportunities and Challenges. *Surf. Sci.* **2002**, *500*, 218−241.

(9) Baughman, R. H.; Zakhidov, A. A.; Heer, W. A. Carbon Nanotubes: The Route Toward Applications. *Science* **2002**, *297*, 787−792.

(10) Wong, K. V.; Bachelier, B. Carbon Nanotubes Used for Renewable Energy Applications and Environmental Protection/Remediation, A Review. *J. Energy Resour. Technol.* **2013**, *136*, 021601−021601−8.

(11) Darkrim, F. L.; Malbrunot, P.; Tartaglia, G. P. Review of Hydrogen Storage by Adsorption in Carbon Nanotubes. *Int. J. Hydrogen Energy* **2002**, *27*, 193−202.

(12) Guldi, D. M.; Rahman, G. M. A.; Zerbetto, F.; Prato, M. Carbon Nanotubes in Electron Donor−Acceptor Nanocomposites. *Acc. Chem. Res.* **2005**, *38*, 871−878.

(13) Popov, V. N. Carbon Nanotubes: Properties and Application. *Mater. Sci. Eng. R* **2004**, *43*, 61−102.

(14) Peigney, A.; Laurent, Ch.; Flahaut, E.; Bacsa, R. R.; Rousset, A. Specific Surface Area of Carbon Nanotubes and Bundles of Carbon Nanotube. *Carbon* **2001**, *39*, 507−514.

(15) Dillon, A. C.; Jones, K. M.; Bekkendahl, T. A.; Kiang, C. H.; Bethune, D. S.; Heben, M. J. Storage of Hydrogen in Single- Walled Carbon Nanotubes. *Nature* **1997**, *386*, 377−379.

(16) Dillon, A. C.; Heben, M. J. Hydrogen Storage Using Carbon Adsorbents. Past, Present and Future. *Appl. Phys. A: Mater. Sci. Process.* **2001**, *72*, 133−142.

(17) Cheng, H. M.; Yang, Q. H.; Liu, C. Hydrogen Storage in Carbon Nanotubes. *Carbon* **2001**, *39*, 1447−1454.

(18) Chen, C. H.; Huang, C. C. Enhancement of Hydrogen Spillover onto Carbon Nanotubes with Defect Feature. *Microporous Mesoporous Mater.* **2008**, *109*, 549−559.

(19) Darkrim, F. L.; Malbrunot, P.; Tartaglia, G. P. Review of Hydrogen Storage by Adsorption in Carbon Nanotubes. *Int. J. Hydrogen Energy* **2002**, *27*, 193−202.

(20) Ye, Y.; Ahn, C. C.; Witham, C.; Fultz, B.; Liu, J.; Rinzler, A. G.; Colbert, D.; Smith, K. A.; Smalley, R. E. Hydrogen Adsorption and Cohesive Energy of Single-Walled Carbon Nanotubes. *Appl. Phys. Lett.* **1999**, *74*, 2307−2309.

(21) Liu, C.; Fan, Y. Y.; Liu, M.; Cong, H. T.; Cheng, H. M.; Dresselhaus, M. S. Hydrogen Storage in Single-Walled Carbon Nanotubes at Room Temperature. *Science* **1999**, *286*, 1127−1129.

(22) Poirier, E.; Chahine, R.; Benard, P.; Cossement, D.; Lafi, L.; Melancon, E.; Bose, T. K.; Désilets, S. Storage of Hydrogen on Single-Walled Carbon Nanotubes and Other Carbon Structures. *Appl. Phys. A: Mater. Sci. Process.* **2004**, *78*, 961−967.

(23) Lawrence, J.; Xu, G. High Pressure Saturation of Hydrogen Stored by Single-Walled Carbon Nanotubes. *Appl. Phys. Lett.* **2004**, *84*, 918−920.

(24) Pradhan, B. K.; Harutyunyan, A. R.; Stojkovic, D.; Grossman, J. C.; Zhang, P.; Cole, M. W.; Crespi, V.; Goto, H.; Fujiwara, J.; Eklund,

P. P. Large Cryogenic Storage of Hydrogen in Carbon Nanotubes at Low Pressures. *J. Mater. Res.* **2002**, *17*, 2209−2216.
(25) Lueking, A. D.; Yang, R. T. Hydrogen Spillover to Enhance Hydrogen Storage. Study of the Effect of Carbon Physicochemical Properties. *Appl. Catal., A* **2004**, *265*, 259−268.
(26) Lupu, D.; Biris, A. R.; Misan, I.; Jianu, A.; Holzhuter, G.; Burkel, E. Hydrogen Uptake by Carbon Nanofibers Catalyzed by Palladium. *Int. J. Hydrogen Energy* **2004**, *29*, 97−102.
(27) Yoo, E.; Gao, L.; Komatsu, T.; Yagai, N.; Arai, K.; Yamazaki, T.; Matsuishi, K.; Matsumoto, T.; Nakamura, J. Atomic Hydrogen Storage in Carbon Nanotubes Promoted by Metal Catalysts. *J. Phys. Chem. B* **2004**, *108*, 18903−18907.
(28) Lachawiec, A. J.; Qi, G. S.; Yang, R. T. Hydrogen Storage in Nanostructured Carbons by Spillover: Bridge-Building Enhancement. *Langmuir* **2005**, *21*, 11418−11424.
(29) Zacharia, R.; Kim, K. Y.; Fazle Kibria, A. K. M.; Nahm, K. S. Enhancement of Hydrogen Storage Capacity of Carbon Nanotubes Via Spillover from Vanadium and Palladium Nanoparticles. *Chem. Phys. Lett.* **2005**, *412*, 369−375.
(30) Kim, H. S.; Lee, H.; Han, K. S.; Kim, J. H.; Song, M. S.; Park, M. S.; Lee, J. Y.; Kang, J. K. Hydrogen Storage in Ni Nanoparticle-Dispersed Multiwalled Carbon Nanotubes. *J. Phys. Chem. B* **2005**, *109*, 8983−8986.
(31) Li, Y. W.; Yang, R. T. Significantly Enhanced Hydrogen Storage in Metal-Organic Frameworks Via Spillover. *J. Am. Chem. Soc.* **2006**, *128*, 726−727.
(32) Krishna Kuma, M.; Ramaprabhu, S. Palladium Dispersed Multiwalled Carbon Nanotube Based Hydrogen Sensor for Fuel Cell Applications. *Int. J. Hydrogen Energy* **2007**, *32*, 2518−2526.
(33) Reddy, A. L. M.; Ramaprabhu, S. Hydrogen Adsorption Properties of Single-Walled Carbon Nanotube-Nanocrystalline Platinum Composites. *Int. J. Hydrogen Energy* **2008**, *33*, 1028−1034.
(34) Suttisawat, Y.; Rangsunvigit, P.; Kitiyanan, B.; Williams, M.; Ndungu, P.; Lototskyy, M. V.; Nechaev, A.; Linkov, V.; Kulprathipanja, S. Investigation of Hydrogen Storage Capacity of Multi-Walled Carbon Nanotubes Deposited with Pd or V. *Int. J. Hydrogen Energy* **2009**, *34*, 6669−6675.
(35) Rather, S.-U.; Nahm, K. S. Hydrogen Uptake of High-Energy Ball Milled Nickel-Multiwalled Carbon Nanotube Composites. *Mater. Res. Bull.* **2014**, *49*, 525−530.
(36) Yildirim, T.; Ciraci, S. Titanium-Decorated Carbon Nanotubes as a Potential High-Capacity Hydrogen Storage Medium. *Phys. Rev. Lett.* **2005**, *94*, 175501−175501−4.
(37) Dag, S.; Ozturk, Y.; Ciraci, S.; Yildirim, T. Adsorption and Dissociation of Hydrogen Molecules on Bare and Functionalized Carbon Nanotubes. *Phys. Rev. B* **2005**, *72*, 155404−15540−8.
(38) Yildirim, T.; Iñiguez, J.; Ciraci, S. Molecular and Dissociative Adsorption of Multiple Hydrogen Molecules on Transition Metal Decorated $C_{60}$. *Phys. Rev. B* **2005**, *72*, 153403−153403−4.
(39) Lee, J. W.; Kim, H. S.; Lee, J. Y.; Kang, J. K. Hydrogen Storage and Desorption Properties of Ni-Dispersed Carbon Nanotubes. *Appl. Phys. Lett.* **2006**, *88*, 143126−143129.
(40) Miao, L.; Bhethanabotla, V. R.; Ossowski, M. M.; Joseph, B. Interactions of Hydrogen with Pd and Pd/Ni Alloy Chain-Functionalized Single Walled Carbon Nanotubes from Density Functional Theory. *J. Phys. Chem. B* **2006**, *110*, 22415−22425.
(41) Durgun, E.; Ciraci, S.; Yildirim, T. Functionalization of Carbon-Based Nanostructures with Light Transition-Metal Atoms for Hydrogen Storage. *Phys. Rev. B* **2008**, *77*, 085405−1−085405−9.
(42) Xiao, H.; Li, S. H.; Cao, J. X. First-Principles Study of Pd-Decorated Carbon Nanotube for Hydrogen Storage. *Chem. Phys. Lett.* **2009**, *483*, 111−114.
(43) López-Corral, I.; Germán, E.; Juan, A.; Volpe, M. A.; Brizuela, G. P. DFT Study of Hydrogen Adsorption on Palladium Decorated Graphene. *J. Phys. Chem. C* **2011**, *115*, 4315−4323.
(44) Zhang, Z.; Li, J.; Jiang, Q. Density Functional Theory Calculations of Metal-Doped Carbon Nanostructures as Hydrogen Storage Systems under Electric Fields: A Review. *Front. Phys.* **2011**, *6*, 162−176.
(45) Tabtimsai, C.; Keawwangchai, S.; Nunthaboot, N.; Ruangpornvisuti, V.; Wanno, B. Density Functional Investigation of Hydrogen Gas Adsorption on Fe-Doped Pristine and Stone−Wales Defected Single-Walled Carbon Nanotubes. *J. Mol. Model.* **2012**, *18*, 3941−3949.
(46) Seenithurai, S.; Kodi Pandyan, R.; Vinodh Kumar, S.; Mahendran, M. $H_2$ Adsorption in Ni and Passivated Ni Doped 4 Å Single Walled Carbon Nanotube. *Int. J. Hydrogen Energy* **2013**, *38*, 7376−7381.
(47) Higgins, S. Regarding Ruthenium. *Nat. Chem.* **2010**, *2*, 1100.
(48) Zhang, Q. H.; Kang, J. C.; Wang, Y. Development of Novel Catalysts for Fischer−Tropsch Synthesis: Tuning the Product Selectivity. *ChemCatChem* **2010**, *2*, 1030−1058.
(49) Yin, S. F.; Xu, B. Q.; Zhou, X. P.; Au, C. T. A Mini-Review on Ammonia Decomposition Catalysts for on-Site Generation of Hydrogen for Fuel Cell Applications. *Appl. Catal., A* **2004**, *277*, 1−9.
(50) Chen, W.; Zuckerman, N. B.; Kang, X. W.; Ghosh, D.; Konopelski, J. P.; Chen, S. W. Alkyne-Protected Ruthenium Nanoparticles. *J. Phys. Chem. C* **2010**, *114*, 18146−18152.
(51) Kang, J.; Deng, W.; Zhang, Q.; Wang, Y. Ru Particle Size Effect in Ru/CNT-catalyzed Fischer−Tropsch Synthesis. *J. Energy Chem.* **2013**, *22*, 321−328.
(52) Liu, J. J.; Bai, P.; Zhao, X. S. Ruthenium Nanoparticles Embedded in Mesoporous Carbon Microfibers: Preparation, Characterization and Catalytic Properties in the Hydrogenation of D-Glucose. *Phys. Chem. Chem. Phys.* **2011**, *13*, 3758−3763.
(53) Chen, J.; Zhu, Z. H.; Wang, S.; Ma, Q.; Rudolph, V.; Lu, G. Q. Effects of Nitrogen Doping on the Structure of Carbon Nanotubes (CNTs) and Activity of Ru/CNTs in Ammonia Decomposition. *Chem. Eng. J.* **2010**, *156*, 404−410.
(54) Liu, X.; Yao, K. X.; Meng, C.; Han, Y. Graphene Substrate-Mediated Catalytic Performance Enhancement of Ru Nanoparticles: A First-Principles Study. *Dalton Trans.* **2012**, *41*, 1289−1296.
(55) Machado, B. F.; Oubenali, M.; Axet, M. R.; NGuyen, T. T.; Tunckol, M.; Girleanu, M.; Ersen, O.; Gerber, I. C.; Serp, P. Understanding the Surface Chemistry of Carbon Nanotubes: Toward a Rational Design of Ru Nanocatalysts. *J. Catal.* **2014**, *309*, 185−198.
(56) Wang, L.; Yang, R. Hydrogen Storage Properties of Carbons Doped with Ruthenium, Platinium and Nickel Nanoparticles. *J. Phys. Chem. C* **2008**, *112*, 12486−12494.
(57) Basri, S.; Kamarudin, S. K.; Daud, W. R. W.; Yaakub, Z. Nanocatalyst for Direct Methanol Fuel Cell (DMFC). *Int. J. Hydrogen Energy* **2010**, *35*, 7957−7970.
(58) Fiordaliso, E. M.; Dahl, S.; Chorkendorff, I. $H_2$ Splitting on Pt/Ru Alloys Supported On Sputtered HOPG. *J. Phys. Chem. C* **2011**, *115*, 25351−25358.
(59) Cerro-Alarcón, M.; Maroto-Valiente, A.; Rodríguez-Ramos, I.; Guerrero-Ruiz, A. Further Insights into the Ru Nanoparticles-Carbon Interactions and their Role in the Catalytic Properties. *Carbon* **2005**, *43*, 2711−2722.
(60) De Moraes, I. R.; Matsubara, E. Y.; Rosolen, J. M. Electrochemical Evidence of Strong Electronic Interaction of PtRu on Carbon Nanotubes with High Density of Defects. *Electrochem. Solid-State Lett.* **2008**, *11*, K109−K112.
(61) Harris, A. G.; Lukehart, C. M.; Gronbeck, H. J. Anchoring of Pt and Pt/Ru To Carbon Nanofibers Studied By Density Functional Theory Calculations. *Carbon* **2014**, *77*, 880−885.
(62) Kohn, W.; Sham, L. J. Self-Consistent Equations Including Exchange and Correlation Effects. *Phys. Rev.* **1965**, *140*, A1133−A1138.
(63) Kresse, G.; Furthmuller, J. Efficiency of Ab-Initio Total Energy Calculations for Metals and Semiconductors Using a Plane Wave Basis Set. *Comput. Mater. Sci.* **1996**, *6*, 15−50.
(64) Perdew, J. P.; Burke, J.; Ernzerhof, M. Generalized Gradient Approximation Made Simple. *Phys. Rev. Lett.* **1996**, *77*, 3865−3868.
(65) Kresse, G.; Joubert, D. From Ultrasoft Seudopotentials to the Projector Augmented-Wave Method. *Phys. Rev. B* **1999**, *59*, 1758−1775.

(66) Blöchl, P. E. Projector Augmented-Wave Method. *Phys. Rev. B* **1994**, *50*, 17953−17979.
(67) Monkhorst, H. J.; Pack, J. D. Special Points for Brillouin-Zone Integrations. *Phys. Rev.* **1976**, *13*, 5188−5192.
(68) Grimme, S. J. Accurate Description of Van der Waals Complexes by Density Functional Theory Including Empirical Corrections. *Comput. Chem.* **2004**, *25*, 1463−1473.
(69) López-Corral, I.; Irigoyen, B.; Juan, A. Bonding in $PdH_2$ and $Pd_2H_2$ Systems Adsorbed on Carbon Nanotubes: Implications for Hydrogen Storage. *Int. J. Hydrogen Energy* **2014**, *39*, 8780−8790.
(70) Baerends, E. J.; Ellis, D. E.; Ros, P. Self-Consistent Molecular Hartree−Fock−Slater Calculations I. The Computational Procedure. *Chem. Phys.* **1973**, *2*, 41−51.
(71) Te Velde, G.; Baerends, E. J. Numerical Integration for Polyatomic Systems. *J. Comput. Phys.* **1992**, *99*, 84−98.
(72) Fonseca Guerra, C.; Visser, O.; Snijders, J. G.; te Velde, G.; Baerends, E. J. *Methods and Techniques in Computational Chemistry*; STEF: Cagliari, Italy, 1995; Vol. *95*, pp 305−395.
(73) Hohenberg, P.; Kohn, W. Inhomogeneous Electron Gas. *Phys. Rev.* **1964**, *136*, B864−B871.
(74) Hoffmann, R. *Solids and Surfaces: A Chemist's View of Bonding in Extended Structures*; VCH: New York, 1988.
(75) *ADF 2.2.1*. Theoretical Chemistry; Vrije Universiteit: Amsterdam, The Netherlands, 1997.
(76) Luna, C. R.; Macchi, C. E.; Juan, A.; Somoza, A. Electronic and Bonding Properties of $MgH_2$−Nb Containing Vacancies. *Int. J. Hydrogen Energy* **2010**, *35*, 12421−12427.
(77) López-Corral, I.; Germán, E.; Juan, A.; Volpe, M. A.; Brizuela, G. P. Hydrogen Adsorption on Palladium Dimer Decorated Graphene: A Bonding Study. *Int. J. Hydrogen Energy* **2012**, *37*, 6653−6665.
(78) Puisto, M.; Nenonen, H.; Puisto, A.; Alatalo, M. Effect of van der Waals Interactions on $H_2$ Dissociation on Clean and Defected Ru (0001) Surface. *Eur. Phys. J. B* **2013**, *86*, 396−396−9.
(79) Knickelbein, M. B.; Koretsky, G. M.; Jackson, K. A.; Pederson, M. R.; Hajnal, Z. Hydrogenated and Deuterated Iron Clusters: Infrared Spectra and Density Functional Calculations. *J. Chem. Phys.* **1998**, *109*, 10692−10700.
(80) Ashman, C.; Khanna, S. N.; Pederson, M. R. Hydrogen Absorption and Magnetic Moment of $Ni_n$ Clusters. *Chem. Phys. Lett.* **2003**, *368*, 257−261.
(81) Bauschlicher, C. W.; Langhoff, S. R. *Transition Metal Hydrides*; VCH: New York, 1992; pp 103−126.
(82) Ge, G.-X.; Yan, H.-X.; Jing, Q.; Luo, Y.-H. Theoretical Study of Hydrogen Adsorption on Ruthenium Clusters. *J. Clust. Sci.* **2011**, *22*, 473−489.
(83) del Rosal, I.; Gutmann, T.; Maron, L.; Jolibois, F.; Chaudret, B.; Walaszek, B.; Limbach, H. H.; Poteau, R.; Buntkowsky, G. DFT 2H Quadrupolar Coupling Constants of Ruthenium Complexes: A Good Probe of the Coordination of Hydrides in Conjuction with Experiments. *Phys. Chem. Chem. Phys.* **2009**, *11*, 5657−5663.
(84) Wang, X.; Andrews, L. Infrared Spectra and Theoretical Calculations for Fe, Ru and Os Metal Hydrides and Dihydrogen Complexes. *J. Phys. Chem. A* **2009**, *113*, 551−563.
(85) Huber, K. P.; Hertzberg, G. *Molecular Spectra and Molecular Structure IV: Constants of Diatomic Molecules*; Van Norstrand Reinhold: New York, 1979.
(86) Durgun, E.; Dag, S.; Bagci, V. M. K.; Gülseren, O.; Yildirim, T.; Ciraci, S. Systematic Study of Adsorption of Single Atoms on a Carbon Nanotube. *Phys. Rev. B* **2003**, *67*, 201401−1−201401−4.
(87) Karami Horastani, Z.; Hashemifar, S. J.; Sayedi, S. M.; Sheikhi, M. H. First-Principles Study of $H_2$ Adsorption on the Pristine and Oxidized (8,0) Carbon Nanotube. *Int. J. Hydrogen Energy* **2013**, *38*, 13680−13686.
(88) Yang, F. H.; Lachawiec, A. J., Jr.; Yang, R. T. Adsorption of Spillover Hydrogen Atoms on Single-Wall Carbon Nanotubes. *J. Phys. Chem. B* **2006**, *110*, 6236−6244.
(89) Reyhani, A.; Mortazavi, S. Z.; Mirershadi, S.; Moshfegh, A. Z.; Parvin, P.; Nozad Golikand, A. Hydrogen Storage in Decorated Multiwalled Carbon Nanotubes by Ca, Co, Fe, Ni and Pd Nanoparticles under Ambient Conditions. *J. Phys. Chem. C* **2011**, *115*, 6994−7001.
(90) Durgun, E.; Dag, S.; Ciraci, S.; Gülseren, O. Energetics and Electronic Structures of Individual Atoms Adsorbed on Carbon Nanotubes. *Phys. Rev. B* **2004**, *108*, 575−582.
(91) Soleymanabadi, H.; Kakemam, K. A DFT Study of $H_2$ Adsorption on Functionalized Carbon Nanotubes. *Phys. E* **2013**, *54*, 115−117.